Open access • Journal Article • DOI:10.1016/J.PHYSD.2008.10.003

Ratchet-induced matter–wave transport and soliton collisions in Bose–Einstein condensates — Source link

Dario Poletti, Dario Poletti, Elena A. Ostrovskaya, Tristram J. Alexander ...+2 more authors

Institutions: Australian National University, National University of Singapore

Published on: 15 Jul 2009 - Physica D: Nonlinear Phenomena (Elsevier)

Topics: Soliton, Bose–Einstein condensate, Ratchet, Matter wave and Optical lattice

Physica D 238 (2009) 1338–1344

Contents lists available at ScienceDirect

Physica D

journal homepage: www.elsevier.com/locate/physd

Ratchet-induced matter–wave transport and soliton collisions in Bose–Einstein condensates

Dario Poletti [a,b], Elena A. Ostrovskaya [a,*], Tristram J. Alexander [a], Baowen Li [b,c], Yuri S. Kivshar [a]

[a] ARC Centre of Excellence for Quantum-Atom Optics and Nonlinear Physics Centre, Research School of Physical Sciences and Engineering, The Australian National University, Canberra ACT 0200, Australia

[b] Department of Physics and Centre for Computational Science and Engineering, National University of Singapore, Singapore 117542, Republic of Singapore

[c] NUS Graduate School for Integrative Sciences and Engineering, 117597, Republic of Singapore

ARTICLE INFO

Article history:
Available online 17 October 2008

PACS:
03.75.Lm
03.75.Kk
05.60.-k

Keywords:
Bose–Einstein condensate
Optical ratchet potential
Matter–wave soliton

ABSTRACT

We study the dynamics of bright matter–wave solitons in a Bose–Einstein condensate with negative scattering length under the influence of a time-periodic ratchet potential. The potential is formed by a one-dimensional bichromatic optical lattice which flashes on and off so that the time average of its amplitude vanishes. Due to the broken space and time-reversal symmetries of the potential, the soliton is transported with a nonzero average velocity. By employing the non-dissipative mean-field model for the matter waves, we study the dependence of the transport velocity on the initial state of the soliton and show how the properties of the individual localized states affect the outcome of their collisions. A useful insight into the transport properties is provided by Hamiltonian theory for the mean field, which treats the extended matter–wave excitation as an effective classical particle.

1. Introduction

The ratchet effect, i.e. rectified average current induced by an asymmetric potential and unbiased zero-mean driving force, appears in both classical and quantum systems and has been extensively studied in dissipative and Hamiltonian regimes [1,2] due to its relevance to biological systems and nanotechnology [3,4]. The theory predicts that, in order for a ratchet to work, the space–time symmetry of the driving potential should be broken [5], and the experiments with cold atoms [6,7] and Bose–Einstein condensates in optical ratchet potentials [8,9] have confirmed this prediction.

The experimental advances in implementing atomic ratchets for Bose–Einstein condensates [8,9] coincide with the growing interest in the effect of interaction on ratchet transport [10–12]. As a physical system with intrinsically present nonlinear interactions due to atomic scattering, a Bose–Einstein condensate (BEC) supports the existence of spatially localized, particle-like collective excitations—*matter–wave solitons*. It is therefore natural to consider the possibility that a ratchet potential can not only provide the means to transport the condensate bulk, but also to control a directed motion of individual matter–wave solitons.

The concept of soliton ratchets was introduced more than ten years ago [13,14] for the driven dynamics of topological (kink) solitons, and those pioneering ideas have been developed further in a number of theoretical studies (see, e.g., Refs. [15–22] to cite a few). In particular, it was shown [14] that the mechanism underpinning the kink ratchet can be understood through the existence of an asymmetric internal mode of the kink soliton that couples, through the damping in the system, to the soliton translational mode. More recently, it was demonstrated that in the damped sine-Gordon equation with periodic nonsinusoidal, additive, and parametric driving forces the ratchet motion of kinks appears as a consequence of a resonance between the oscillations of the momentum and the width of the kink [22]. These results follow from the topological nature of this type of soliton possessing a finite rest mass.

Unlike the ratchet dynamics of kinks, the effect of the ratchet potential on bright non-topological solitons has received very little attention. Until recently, the research in this direction was restricted to discrete dissipative nonlinear systems [23]. Recently we have studied the ratchet motion of bright solitons in Bose–Einstein condensates with attractive atomic interactions in a weak "flashing" optical lattice and revealed many novel features of their induced dynamics [24]. Importantly, we have shown that both the ratchet effect and soliton directed transport are observed in this system even in the absence of losses (damping), which sets it apart from previously studied dissipative nonlinear systems [23], and also indicates that the mechanism for ratchet transport of

* Corresponding author.
E-mail address: ost124@rsphysse.anu.edu.au (E.A. Ostrovskaya).

0167-2789/$ – see front matter © 2008 Elsevier B.V. All rights reserved.
doi:10.1016/j.physd.2008.10.003

bright solitons differs dramatically from that of kinks. Although focused on BEC solitons, our work is of general importance as a first, to our knowledge, study of the ratchet dynamics of a general class of non-topological, non-dissipative solitons described by a continuous Gross–Pitaevskii (or nonlinear Schrödinger) equation. In this paper we briefly overview the main theoretical results as well as study in more detail the effect of the flashing ratchet potential on the dynamics of a single matter–wave soliton and soliton scattering.

The paper is organized as follows. First, in Section 2 we introduce our mean-field model, which is given by a Gross–Pitaevskii equation with a time-varying periodic potential. In Section 3 we present details of the effective particle approximation used to analyze the soliton dynamics.Then, in Section 4 we describe the dynamics of a single soliton in the presence of the flashing ratchet and investigate the main features of its cumulative and average velocity. Section 5 is devoted to the study of ratchet-driven soliton collisions where we consider several cases including the binary interactions between solitons of different effective masses, as well as multiple soliton collisions. Section 6 discusses the relevant parameters of the corresponding physical system, and Section 7 concludes the paper.

2. Mean-field model

To simplify the modeling of the system, we consider a strongly elongated condensate cloud [25] subjected to a flashing one-dimensional optical lattice (see, e.g., [10]). As long as the energy of the longitudinal excitations is not sufficient to excite the transverse modes of the condensate, the system can be treated as one-dimensional [26] and described by the Gross–Pitaevskii (GP) equation:

$$\mathrm{i}\frac{\partial\Psi}{\partial t}+\frac{1}{2}\frac{\partial^2\Psi}{\partial x^2}+|\Psi|^2\Psi-V(x,t)\Psi=0, \tag{1}$$

where the lattice potential,

$$V(x,t)=V_0 f(t)\left[\cos(x)+\cos(2x+\phi)\right], \tag{2}$$

is driven biperiodically: $f(t)=\sin(\omega t)+\sin(2\omega t)$, and V_0 depends on the intensity of the laser beams forming the lattice. The space inversion symmetry of this potential ($x\to -x+\tilde{x}$) is broken for $\phi\neq 0,\pi$. In its time-dependent form, the potential (2) is not invariant with respect to the time inversion ($t\to -t+\tilde{t}$). The importance of breaking these symmetries for the ratchet dynamics will be discussed in the following sections.

The dimensionless form of Eq. (1) is derived by using the following energy, length, and frequency scales: $E_0=\hbar^2k^2/m$, $a_0=1/k$, and $\omega_0=\hbar k^2/m$, where m is the mass of the atoms, and k is the wavevector of the optical lattice. The dimensionality reduction procedure, valid for a quasi-one-dimensional trapping geometry considered here, allows us to separate the condensate wavefunction into its transverse and longitudinal components [26]: $\psi_{3D}(x,y,z)=\psi_{1D}(x)\Phi(y,z)$, where $\Phi(y,z)$ is the ground state wavefunction, of the two-dimensional harmonic trap with the transverse trapping frequency $\omega_\perp$. The dimensionless wavefunction Ψ in Eq. (1) relates to ψ_{1D} as follows: $\Psi=\psi_{1D}\sqrt{g_{1D}}$, where $g_{1D}=2(a_s\omega_\perp)/(a_0\omega_0)$ is the renormalized coefficient that characterizes the s-wave interaction of the condensate atoms with the scattering length a_s. The norm of the dimensionless wavefunction, $N=\int|\Psi|^2\mathrm{d}x$, is directly related to the actual number of atoms in the condensate or a localized excitation: $\mathcal{N}=N/g_{1D}$. In the case of a localized matter–wave soliton it may be referred to as its effective mass [27].

3. Effective particle approach

To understand the effect of the weak flashing potential on the dynamics of a collective excitation in the BEC, we consider a single localized excitation in the form of a one-dimensional bright soliton. In the absence of perturbations, the shape of the soliton is defined by self-focusing of the matter–wave due to the attractive interaction between the atoms, and is given by the exact solution of the one-dimensional GP equation:

$$\Psi(x,0)=\frac{N}{2}\,\mathrm{sech}\left[\frac{N}{2}(x-X_0)\right]. \tag{3}$$

Here $X_0\equiv X(0)$ is the initial position of the soliton's center of mass defined as:

$$X(t)=\frac{1}{N}\int_{-\infty}^{\infty}\Psi^*(x,t)x\Psi(x,t)\mathrm{d}x. \tag{4}$$

The Hamiltonian description of the mean field [28] allows us to write an effective energy integral associated with the equation of motion Eq. (1):

$$H(x,t)=\int_{-\infty}^{\infty}\left[\frac{1}{2}\left|\frac{\partial\Psi}{\partial x}\right|^2+\frac{|\Psi|^4}{2}-V|\Psi|^2\right]\mathrm{d}x. \tag{5}$$

If the ratchet potential is weak, the soliton shape is preserved during its evolution and its dynamics is described by the motion of the center of mass. In this case, the extended collective excitation can be treated as a classical particle [29] that moves in the effective potential,

$$\begin{aligned}V_{\mathrm{eff}}(t)&=\frac{1}{N}\int_{-\infty}^{\infty}|\Psi(x,0)|^2V(x,t)\mathrm{d}x\\&=\frac{\pi V_0}{N}f(t)\left[\frac{\cos X}{\sinh(\pi/N)}+2\frac{\cos(2X+\phi)}{\sinh(2\pi/N)}\right].\end{aligned} \tag{6}$$

Using Eq. (6) the soliton velocity can be obtained by integrating the classical equation of motion for the soliton center of mass [29,30],

$$\frac{\mathrm{d}^2X}{\mathrm{d}t^2}=-\frac{\partial V_{\mathrm{eff}}}{\partial X}. \tag{7}$$

The effective particle approach (EPA) allows us to make intuitive predictions about the transport properties of the soliton as an effective classical particle in the external potential $V_{\mathrm{eff}}(t,x)$. It can be seen that if the lattice potential is a simple single-period function of space and time, $V(x,t)\sim\cos(x)\sin(\omega t)$, then due to the symmetries of the potential the dynamical system (1) is invariant with respect to the symmetry transformations: $x\to -x+\tilde{x}$, $t\to -t+\tilde{t}$. Such transformations simultaneously change the sign of the soliton velocity, $v(t)=\mathrm{d}X/\mathrm{d}t$, and hence the velocity averaged over all initial conditions in time and space is zero. In contrast, when both of these symmetries are broken, as is the case with the potential (2), according to the symmetry analysis [5], we expect that a nonzero average velocity and hence a directed transport of matter–wave solitons may occur under the influence of the driving. The significance of the symmetry breaking and the dependence on the initial conditions are examined in detail below.

We note that the instantaneous shape of the effective potential, V_{eff}, shown in Fig. 1 (red solid line) becomes closer to the asymmetric shape of the optical lattice, $V(x,t)$, as N grows and the soliton becomes more localized. Therefore, the spatial asymmetry of the ratchet potential is most pronounced for strongly localized excitations, containing a large number of atoms, and as a result

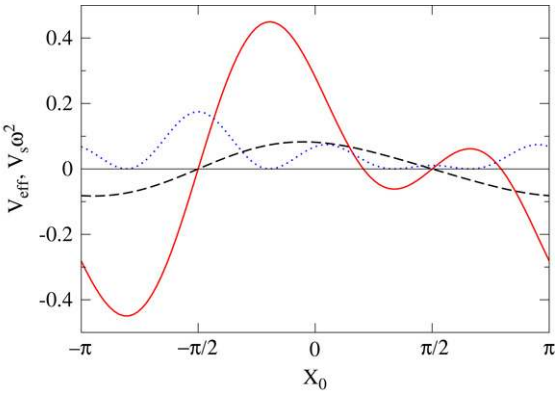

Fig. 1. Effective potential V_{eff} at $f(t) = 1$ vs. initial position of soliton's center of mass, X_0, for $N = 1$ (black dashed line) and $N = 5$ (red solid line), and the time-averaged potential V_s at $N = 5$ (blue dotted line). Parameters are: $V_0 = 0.3$, $\phi = \pi/2, \omega = 10$.

we expect larger values of time-averaged (cumulative) velocity defined as:

$$\bar{v} = \lim_{T\to\infty} \frac{1}{T - t_0} \int_{t_0}^{T} \frac{\mathrm{d}X}{\mathrm{d}t} \mathrm{d}t. \tag{8}$$

In contrast, for small N the second term in (6) becomes exponentially smaller than the first one, and hence the effective potential becomes practically symmetric, as demonstrated by a black dashed line in Fig. 1. The loss of spatial asymmetry should translate to the suppression of the average current for weakly localized solitons with low peak densities. At large driving frequencies the dynamics of the classical particle in the effective potential, V_{eff}, is regular. There are two basic types of trajectories: transporting (in position) and non-transporting or oscillating, whereas the momentum always remains bounded [24]. The soliton engaged in the near-ballistic motion will then exhibit acceleration and deceleration on a short time scale, as shown in Fig. 2(b), with a constant non-zero average momentum which will result in the overall transport [see Fig. 2(a)]. The simulations of ballistic motion in Fig. 2 are performed with periodic boundary conditions, however we make sure that the tails of the soliton never overlap. From these simulations we infer that the typical soliton motion is characterized by two different time scales, $T_0 = 2\pi/\omega$, the period of fast driving, and T_s, the time of slow motion. Following the standard averaging technique for rapidly driven classical nonlinear systems (see [31,32] and also [5]) we decompose the motion of the center of mass into a sum of slowly and rapidly varying parts, $X(t) = X_s(t) + \xi(t)$, where the mean value of the fast oscillations, $\xi(t)$, is zero over the period of driving. Substituting this decomposition into Eq. (7), expanding the right hand side in powers of ξ, and performing the averaging over T_0, we obtain in the lowest order of the small parameter of the system, $\varepsilon = T_0/T_s$, the explicit expression for the fast variable:

$$\xi(t) = -g(X_s)\frac{V_0\pi}{N\omega^2}\left[\sin(\omega t) + \frac{1}{4}\sin(2\omega t)\right], \tag{9}$$

and an equation of motion for the slow variable:

$$\frac{\mathrm{d}v_s}{\mathrm{d}t} = \frac{\mathrm{d}^2X_s}{\mathrm{d}t^2} = -\frac{\mathrm{d}V_s}{\mathrm{d}X_s}. \tag{10}$$

The conservative effective potential of the slow motion in Eq. (10) is:

$$V_s(X_s) = \frac{5}{16}\left(\frac{V_0\pi}{N\omega}\right)^2 g^2(X_s), \tag{11}$$

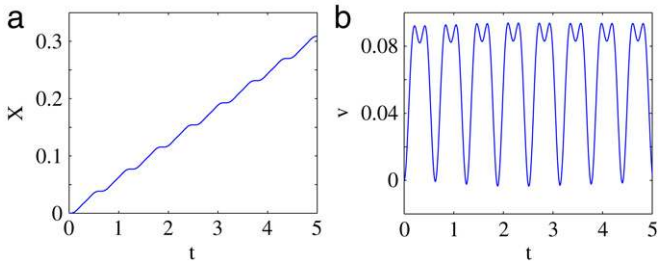

Fig. 2. (a) Soliton center of mass position and (b) velocity as a function of time corresponding to the near-ballistic motion. Parameters are: $V = 0.3, \phi = \pi/2$, $\omega = 10, t_0 = 0$.

where

$$g(X_s) = s_1 \sin X_s + s_2 \sin(2X_s + \phi), \tag{12}$$

and $s_1 = 1/\sinh(\pi/N), s_2 = 4/\sinh(2\pi/N)$. The typical form of V_s is shown in Fig. 1 (blue dotted line).

As pointed out in [5], all the asymmetries of the system are now concealed not only in the spatial asymmetry of V_s (see Fig. 1) but also in the initial conditions (at $t = t_0$) for the slow variable and its velocity:

$$\begin{aligned} X_s(t_0) &= X_0; \\ v_s(t_0) &= g(X_0)\frac{V_0\pi}{N\omega}\left[\cos(\omega t_0) + \frac{1}{2}\cos(2\omega t_0)\right] \end{aligned} \tag{13}$$

where we assumed, as is the case throughout this paper, that the soliton is initially at rest. Given these initial conditions, Eq. (10) can be integrated once to give:

$$v_s^2 = v_s^2(t_0) + 2\left[V_s(X_0) - V_s(X_s)\right]. \tag{14}$$

As we will demonstrate in the following sections, even though the main Eqs. (10) and (13) of the time-averaged EPA do not offer an analytical dependence $v_s(t; X_0, t_0)$ in a simple form, they nevertheless allows us to make intuitive predictions about the properties of the soliton current in the ratchet potential, which is not easy to do with the aid of the GP model (1) or EPA alone.

4. Dynamics of a single soliton

To describe the properties of the non-zero soliton current caused by the ratchet potential, we first consider the *cumulative velocity* of the single soliton. As can be seen in Fig. 3, where we have used $T \approx 10^3 \times 2\pi/\omega, X_0 = 0$ and $t_0 = 0$, the EPA predictions (dashed line) obtained by integrating Eq. (7) are in qualitative agreement with the numerical results obtained from the GP model (solid line). As shown in Fig. 3, for a given initial position of a soliton, its cumulative velocity is a function of its norm, N. Clearly as $T \to \infty$ the main contribution to the cumulative velocity comes from near-ballistic trajectories, for which $v(t) = v_s(t) \approx v_s(t_0)$. Consequently, the cumulative velocity for large N can be estimated from the equations for the slow soliton motion to be $\bar{v} = v_s(t_0) = 6V_0\pi/(N\omega)\sinh^{-1}(2\pi/N)$, which is in good agreement with numerical solutions (dotted line in Fig. 3). As $N \to \infty$ the velocity of the ballistic motion tends to a constant value, which for the parameters in Fig. 3 is equal to $v_s(0) \approx 3V_0/\omega = 0.09$.

In the absence of the transporting motion in the system the cumulative velocity is zero. This is reflected in the sharp cut-off for the cumulative velocity at low values of N seen in Fig. 3. According to the time-averaged EPA theory, the soliton acquires transporting motion if its initial energy, E_s, is greater than the peak amplitude of the effective confining potential $V_s^{\max}$, otherwise the soliton oscillates. Given the explicit form of the effective potential for the

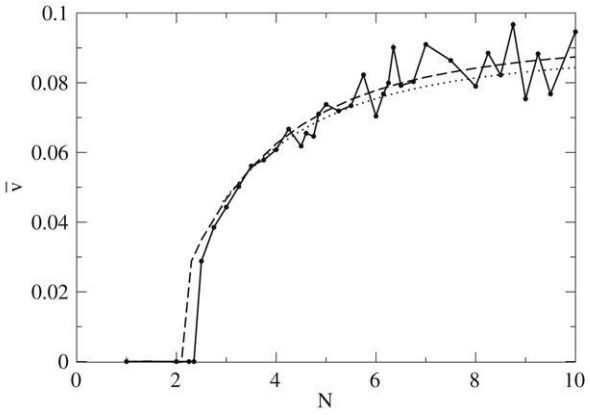

Fig. 3. Cumulative velocity $\bar{v}$ vs. norm of the BEC wavefunction, N, calculated using Eq. (1) (solid line), Eq. (7) (dashed), and $v_s(t_0)$ given by Eq. (13) for $N \leq 3$ (dotted); $\bar{v} = 1$ corresponds to 3.5 mm/s. Parameters are: $V = 0.3$, $\phi = \pi/2$, $\omega = 10$, $X_0 = 0$, $t_0 = 0$.

slow motion V_s and the soliton velocity, $v_s(t_0)$, the critical ratio for $t_0 = 0$ and $\phi = \pi/2$ is:

$$\frac{E_s}{V_s^{\max}} = \frac{23}{5}\left(\frac{s_1 \sin X_0 + s_2 \cos 2X_0}{s_1 + s_2}\right)^2. \tag{15}$$

The solution of the equation $E_s = V_s^{\max}$ with respect to N determines the cut-off value of the norm, which for the case $X_0 = 0$ is $N_{\rm cr} = 2.13$ (c.f. Fig. 3).

As suggested by Eq. (15), the type of soliton motion (transporting or oscillating) will strongly depend not only on N, but also on its initial position relative to the lattice potential. The illustration of this drastic dependence is given in Fig. 4, where solitons with the same $N = 2$ but different X_0 are shown to be trapped (a, b) or transported (d) by the flashing lattice. We note that Eq. (15) correctly predicts the behavior of the soliton for the given X_0 in all cases, giving $E_s/V_s^{\max} = (23/5)s_2^2/(s_1+s_2)^2 < 1$ in the case (a), $E_s/V_s^{\max} = (23/5)(s_1-s_2)^2/(s_1+s_2)^2 \ll 1$ in the case (b), and $E_s/V_s^{\max} = 23/5 > 1$ in the transporting case (d).

In addition, transported solitons starting off at different positions, X_0, can move in different directions, as shown in Fig. 4(c, d). The direction and speed of the transport as a function of X_0 and N are readily predicted by the expression for the initial velocity $v_s(t_0)$ of the slow motion (13). The qualitative correspondence between the value of the initial velocity $v_s(t_0)$ and that calculated by numerical solution of the GP model (1) is clearly illustrated in Figs. 4(c, d) and 5.

The detailed examination of the dependence of the cumulative velocity $\bar{v}$ on the initial position of the center of mass, X_0, shows that the predictions of the EPA (7) and the numerical solution of the GP model (1) disagree for small values of N. As shown in Fig. 6(a, b) for both $N = 1$ and $N = 2$ the numerical results show that the soliton has either no cumulative velocity, or moves in only one direction. In contrast, the cumulative velocity calculated using the equation of motion (7) arising from the EPA is almost symmetric with respect to $X_0 = 0$ as expected in the limit of small N due to the symmetry of the effective potential (see Fig. 1). These discrepancies are due to the fact that for $N < 2.5$ the soliton's size is comparable with or larger than a period of the optical lattice, and hence it is more accurately described as a wavepacket than an effective particle.

For larger values of norm, e.g., $N \approx 5$, corresponding to a strongly localized matter–wave soliton, the dynamics is well described by the EPA. Accordingly, in Fig. 6(c) we see a good agreement between the numerical solution of the GP model (1) and the EPA equation (7) in the details of the cumulative velocity dependence on X_0.

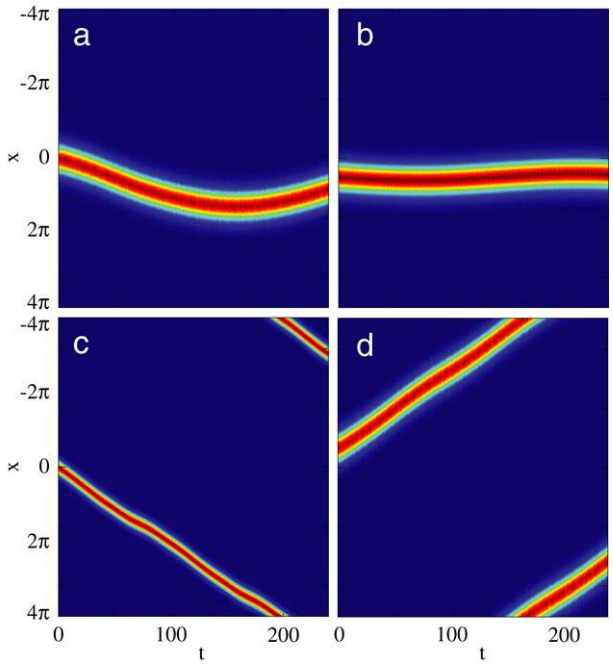

Fig. 4. Density plots of the mean-field evolution, $|\Psi(x,t)|^2$, shown for (a) $N = 2$ and $X_0 = 0$, (b) $N = 2$ and $X_0 = \pi/2$, (c) $N = 4$ and $X_0 = 0$, and (d) $N = 2$ and $X_0 = -\pi/2$ Parameters are: $V = 0.3$, $\phi = \pi/2$, $\omega = 10$, $t_0 = 0$.

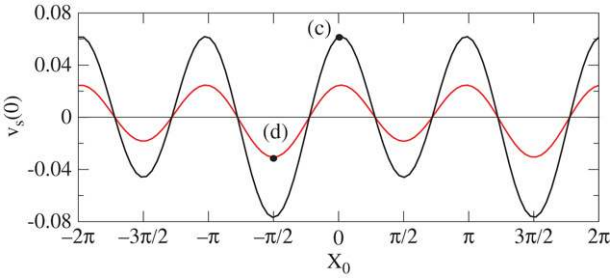

Fig. 5. Initial velocity of the soliton center of mass, $v_s(t_0)$ as a function of initial position for $N = 4$ (black) and $N = 2$ (red). The marked points correspond to the ballistic motion shown in Fig. 4(c, d). Parameters are: $V = 0.3$, $\phi = \pi/2$, $\omega = 10$, $t_0 = 0$.

5. Average current

Despite the strong dependence of the dynamics on the initial position of the soliton, since the space inversion symmetry of the lattice is broken, we can expect that averaging over all initial soliton positions, X_0, will lead to a nonzero averaged velocity:

$$\langle \bar{v} \rangle_{X_0} = \frac{1}{2\pi}\int_{-\pi}^{\pi} \bar{v}\,dX_0, \tag{16}$$

and thus signal the true ratchet effect. Indeed, even the rough analytical estimate of the soliton velocity obtained from (14):

$$\bar{v}_s \sim \sqrt{\frac{17}{8}}\frac{V_0\pi}{N\omega}\frac{g^3(X_0)}{g^2(X_0) + (5/68)(s_1^2+s_2^2)}, \tag{17}$$

is non-zero when averaged over X_0. However, this expression underestimates the absolute value of the cumulative (and hence averaged) velocity and the numerical solution of the equations of motion (7) and (10) can be employed to obtain more accurate dependence. In Fig. 7 we plot the soliton velocity calculated using the model GP equation, EPA (7) and time-averaged EPA (10) averaged over all initial positions as a function of the number of atoms. Indeed we observe that the average velocity is non-zero and

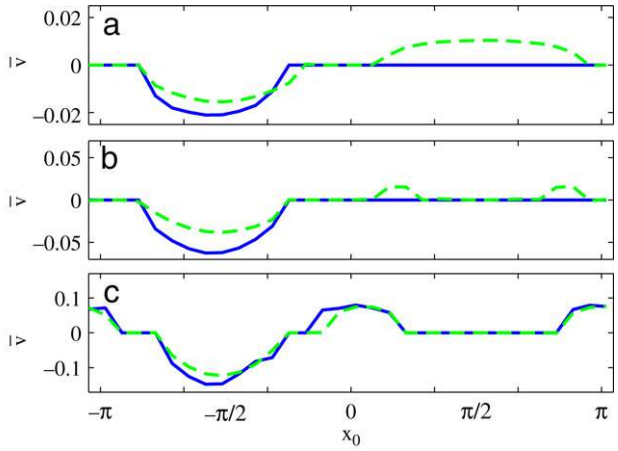

Fig. 6. Cumulative velocity, $\bar{v}$, vs. soliton initial position, X_0, for (a) $N = 1$; (b) $N = 2$; (c) $N = 5$; calculated from the numerical solution of the GP equation (solid line) and EPA (dashed). Parameters are: $V_0 = 0.3$, $\phi = \pi/2$, $\omega = 10$, $t_0 = 0$.

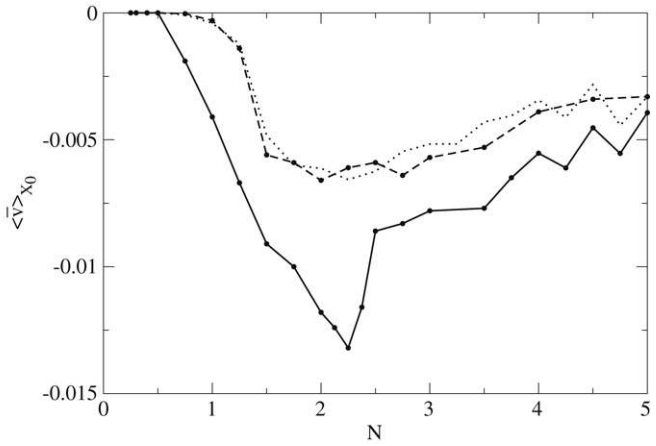

Fig. 7. Average velocity $\langle\bar{v}\rangle$ vs. number of atoms in the soliton, N, calculated using the GP model (solid line), EPA (dashed), and time-averaged EPA (dotted). Parameters are: $V_0 = 0.3$, $\phi = \pi/2$, $\omega = 10$, $t_0 = 0$.

therefore the ratchet transport is present in this system, as long as the number of atoms (or the norm, N) of the solitons is large.

As expected and seen in Fig. 7, the EPA results obtained by solving Eq. (7) and numerical solution of Eq. (1) agree for large values of N, but disagree both on the onset of the ratchet effect and on its magnitude at small N. In particular, as demonstrated in Fig. 6(a, b), for $N < 2.5$ a soliton attains a much larger average velocity than that predicted by the EPA theory due to the fact that the potential experienced by effective particle, V_{eff}, loses its spatial asymmetry. It is especially remarkable that the ratchet works much better for a weakly localized soliton than it does for a strongly-localized particle-like excitation, achieving larger average velocities in the case when the extended nature of the excitation cannot be ignored.

We note that the time-averaged EPA (10) [dotted line in Fig. 7] makes a correct prediction about the order of magnitude of the nonzero average current for smaller N, but is not reliable for larger N, where chaotic trajectories occur for certain X_0.

Finally, we discuss the the importance of the time-reversal symmetry breaking for the ratchet dynamics of a matter–wave soliton. So far, we have discussed the averaging over the initial positions of the soliton, X_0 assuming that the soliton is loaded into the lattice at the time $t_0 = 0$. However, in an experiment both X_0 and t_0 would be difficult to control. Therefore any attempt to detect an average current would involve the averaging over many

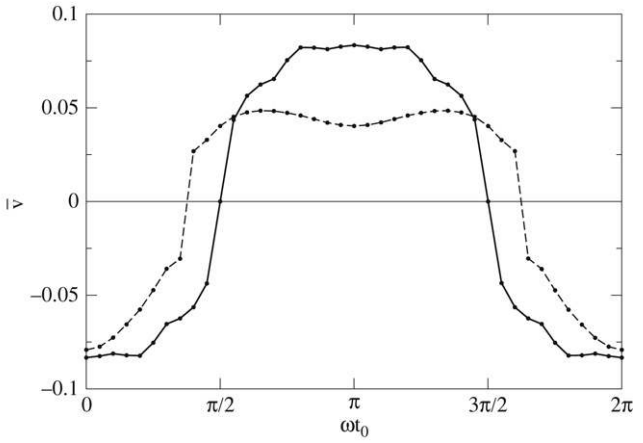

Fig. 8. Cumulative velocity, $\bar{v}$, vs. initial time, t_0, calculated using the GP model (1) and the time-varying lattice amplitude, $f(t)$, which includes either one (solid line) or two (dashed) harmonics. Parameters are: $V_0 = 0.3$ for a biperiodic and $V_0 = 0.528$ for single-harmonic driving, $\omega = 10$, $N = 2.5$, and $X_0 = -\pi/2$.

experimental realizations, i.e. effectively over both X_0 and t_0. Fig. 8 shows the cumulative velocity of the soliton computed using the GP model over the range of initial conditions at t_0 sampled over a single driving period. Importantly when the time-reversal (shift) symmetry $\{t \to -t + \pi/\omega,\ \Psi \to \Psi^*\}$ is preserved, as is the case for a single-harmonic driving with $f(t) = \sin(\omega t)$, the dependence $\bar{v}(t_0)$ is completely symmetric (solid line in Fig. 8) and averaging over all t_0 produces zero total current ($\langle\bar{v}_s\rangle_{t_0} = -1.75 \times 10^{-5}$ in Fig. 8). In contrast, the biperiodic in time potential (2) with $f(t) = \sin(\omega t) + \sin(2\omega t)$ breaks the symmetry and produces a non-zero average velocity ($\langle\bar{v}_s\rangle_{t_0} = 5.14 \times 10^{-3}$ in Fig. 8).

Remarkably, this result can be also confirmed in the time-averaged EPA picture, where the potential confining the effective particle is both time-independent and does not depend on t_0. Instead the critical information about the time-dependence of driving and hence time-reversal (shift) symmetries in this approach is contained in the initial condition $v_s(t_0)$ [see Eq. (13)]. We have checked that averaging of the cumulative velocity $\bar{v}_s$ over all t_0 with the parameters used to produce Fig. 8 yields $\langle\bar{v}_s\rangle_{t_0} = -2 \times 10^{-6}$ and $\langle\bar{v}_s\rangle_{t_0} = 5.37 \times 10^{-3}$ for a single-harmonic and biperiodic $v_s(t_0)$, respectively.

6. Ratchet-induced soliton collisions

The dependence of the soliton velocity on N means that dissimilar solitons placed at the same positions (i.e. at $X_0 + 2\pi m$, where m is an integer) relative to the ratchet potential will move at different speeds and engage in collisions. Conversely, if the solitons are identical, collisions can occur only if they have different initial positions in the lattice (and therefore different cumulative velocities). The difference between the two scattering scenarios is in the interaction energy, which for a pair of solitons 1 and 2 is proportional to $N_1 N_2$ (see, e.g., [27]). For a fixed $N_1 \geq N_2$, the interaction is stronger in the case of solitons with equal norms. This leads to different scattering patterns in the cases of $N_2 \neq N_1$ and $N_1 = N_2$.

A single collision event is nearly elastic in the case of strongly dissimilar solitons. The driving has little effect on the soliton collisions because of its small amplitude and fast variation, and each collision event leads to small incremental changes in the soliton's position in the phase space. In order to detect the effect of the ratchet potential, multiple soliton collisions should be realized. This would be possible in an experiment if the ratchet potential was combined with a toroidal trap [33]. Numerically, toroidal geometry is easily simulated by adopting periodic boundary

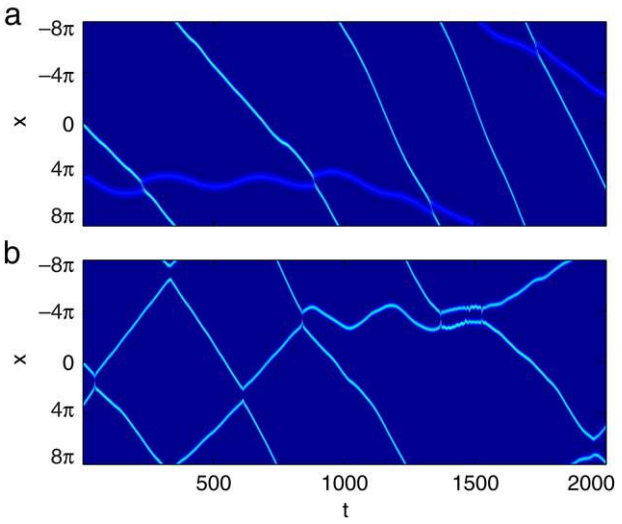

Fig. 9. (a) Collision between two soliton, one with $N = 4$ with initial position $X_0 = 0$ and the other one with $N = 2.2$ and initial position $X_0 = 4\pi$. (b) Collision between two soliton with $N = 4$ located at $X_0 = 0$ and $x_0 = 3\pi + 1.2$. Parameters are: $V_0 = 0.3$. $\phi = \pi/2$, $\omega = 10$, $t_0 = 0$.

conditions. As can be seen in Fig. 9(a), in a multiple scattering process of in-phase solitons, a larger moving soliton can induce the transport of a smaller soliton which would otherwise not be transported by the ratchet. This is due to the fact that incremental changes in the soliton's position and momentum eventually move the smaller soliton from a non-transporting to a transporting trajectory in the phase space.

In the case of identical in-phase solitons, each collision event can induce a sudden shift from a non-transporting to a transporting trajectory in the soliton's phase space, and vice versa. This is evident in Fig. 9(b) where we can see dramatic changes in the soliton velocities after collisions. In this scenario, the spatial shift that solitons acquire during each collision may lead to an effective averaging over X_0 after multiple collisions. As a result, a nonzero average density current can, in principle, be observed for a sufficiently large number of collisions or for a sufficiently large number of interacting solitons. An example of this effect is shown in Fig. 10(a), which displays the collision of seven solitons with different norms. Such a distribution of solitons can be prepared, for example, if a ground state of an attractive condensate in a harmonic trap is fragmented by a deep optical lattice. We show the details of the profiles of the wavepackets at time $t = 0$ [Fig. 10(b)], $t = 300$ [Fig. 10(c)] and $t = 600$ [Fig. 10(d)]. One can see that the collision event strongly affects the solitons with large peak densities which are strongly transported by the ratchet and as a result spatially separated from the smaller wavepackets. This suggests the possibility of spatial filtering of solitons by soliton particle number.

7. Physical parameters

To relate our dimensionless quantities to the typical experimental parameters, we consider, as an example, the experimental setup of Ref. [25] employed to observe a bright matter–wave soliton in a strongly elongated ^{7}Li condensate cloud. In order to observe the one-dimensional soliton, the scattering length of ^{7}Li was modified to be $a_s \approx -0.21$ nm, and the condensate was trapped in a quasi-one-dimensional atomic waveguide with $\omega_\perp = 2\pi \times 710$ Hz. We note that, for this value of the transverse frequency, the chemical potential corresponding to a BEC soliton is

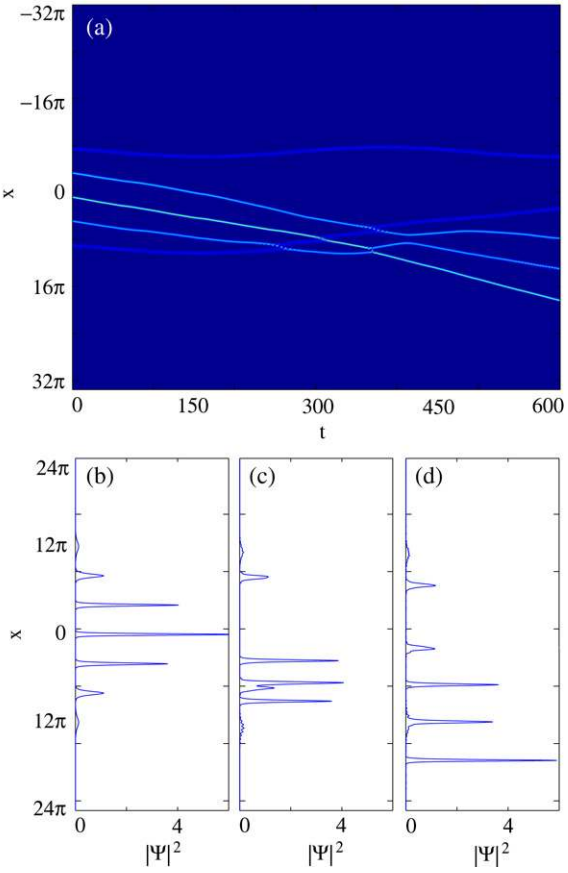

Fig. 10. (a) Density plot of the mean-field evolution, $|\Psi(x, t)|^2$ of 7 solitons with $N = 5$ and $X_0 = 0$, $N \approx 4.01$ and $x_0 = \pm 4\pi$, $N \approx 2.1$ and $X_0 = \pm 8\pi$ and $N \approx 0.7$ and $X_0 = \pm 12\pi$. (b)-(c)-(d) Density of the wave-function $|\Psi|^2$ versus x respectively at time $t = 0$, $t = 300$ and $t = 600$. Parameters are: $V = 0.3$, $\phi = \pi/2$, $\omega = 10$, $t_0 = 0$.

always smaller than the transverse excitation energy, which justifies the dimensionality reduction in the mean-field model.

To realize an optical ratchet potential in a similar setup, an additional optical lattice can be superimposed along the waveguide axis. The realization of the flashing lattice is within current experimental capabilities and the stationary form of the potential (2) was recently realized in the experiments with ultracold rubidium vapor in a Fourier-synthesized optical lattice [34]. If the lattice is formed by light beams derived from a CO_2 laser with wavelength $\lambda = 10.62$ μm, crossed at an angle $\theta = 38°$, then our scaling units of length and frequency take the values $a_0 = \lambda/[4\pi \sin(\theta/2)] = 2.52\,\mu$m and $\omega_0 = 2\pi \times 224$ Hz. A stable bright soliton typically created in the experiment [25] contains $\mathcal{N} \approx 5 \times 10^3$ atoms, which corresponds to the soliton norm $N \approx 2.62$ in our units. We note that, due to the nature of our scaling, the same value of the atom number, $\mathcal{N}$, may correspond to larger or smaller values of a_0 (and hence N), depending on the angle θ.

8. Conclusions

We have studied the dynamics and transport of bright matter–wave solitons in a weak flashing optical ratchet potential. The important feature of the ratchet-induced transport is the dependence of the soliton cumulative velocity on both number of atoms and the initial position of the soliton. For small atom numbers, the soliton transport occurs in one direction only, while larger solitons may be transported in either direction. As a result, the averaging over all initial positions results in a strong ratchet

effect for solitons with small peak densities. The results obtained by direct numerical integration of the one-dimensional mean-field model show good qualitative agreement with the effective-particle approximation. However, the ratchet works best for solitons whose width is comparable with the spatial period of the perturbing potential, in the regime where the effective particle approximation is less applicable.

Finally, we have investigated the scattering of the matter–wave solitons moving under the influence of a ratchet potential. Depending on the size of the interacting solitons, their collisions can cause either gradual or instantaneous transitions between transporting and non-transporting trajectories in the phase space. We have demonstrated that for multiple solitons of different sizes, initially formed in a harmonically trapped condensate, this effect could result in directed transport or spatial filtering of solitons.

Acknowledgments

The authors gratefully acknowledge discussions with S. Denisov and M. Salerno. This work is supported by the Australian Research Council (ARC) through the Discovery and Centre of Excellence research projects.

References

[1] P. Reimann, M. Grifoni, P. Hänggi, Phys. Rev. Lett. 79 (1997) 10;
J. Lehmann, S. Kohler, P. Hänggi, A. Nitzan, Phys. Rev. Lett. 88 (2002) 228305;
G.G. Carlo, G. Benenti, G. Casati, D.L. Shepelyansky, Phys. Rev. Lett. 94 (2005) 164101.
[2] H. Schanz, M.F. Otto, R. Ketzmerick, T. Dittrich, Phys. Rev. Lett. 87 (2001) 070601;
T.S. Monteiro, P.A. Dando, N.A.C. Hutchings, M.R. Isherwood, Phys. Rev. Lett. 89 (2002) 194102;
S. Denisov, L. Morales-Molina, P. Hänggi, S. Flach, Phys. Rev. A 75 (2007) 063424.
[3] R.D. Astumian, P. Hänggi, Phys. Today 55 (11) (2002) 33.
[4] P. Reimann, Phys. Rep. 361 (2002) 57.
[5] S. Flach, O. Yevtushenko, Y. Zolotaryuk, Phys. Rev. Lett. 84 (2000) 2358.
[6] R. Gommers, S. Denisov, F. Renzoni, Phys. Rev. Lett. 96 (2006) 240604.
[7] P.H. Jones, M. Goonasekera, D.R. Meacher, T. Jonckheere, T.S. Monteiro, Phys. Rev. Lett. 98 (2007) 073002.
[8] M. Sadgrove, M. Horikoshi, T. Sekimura, K. Nakagawa, Phys. Rev. Lett. 99 (2007) 043002.
[9] I. Dana, V. Ramareddy, I. Talukdar, G.S. Summy, Phys. Rev. Lett. 100 (2008) 024103.
[10] D. Poletti, G. Benenti, G. Casati, B. Li, Phys. Rev. A 76 (2007) 023421.
[11] L. Morales-Molina, S. Flach, New J. Phys. 10 (2007) 013008.
[12] O. Romero-Isart, J.J. Garcia-Ripoll, Phys. Rev. A 76 (2007) 052304.
[13] F. Marchesoni, Phys. Rev. Lett. 77 (1996) 2364.
[14] M. Salerno, N. Quintero, Phys. Rev. E 65 (2002) 025602.
[15] M. Salerno, Y. Zolotaryuk, Phys. Rev. E 65 (2002) 056603.
[16] C.R. Willis, M. Farzaneh, Phys. Rev. E 69 (2004) 056612.
[17] L. Morales-Molina, F.G. Mertens, A. Sánchez, Eur. Phys. J. B 37 (2004) 79.
[18] N.R. Quintero, B. Sánchez-Rey, M. Salerno, Phys. Rev. E 72 (2005) 016610.
[19] L. Morales-Molina, F.G. Mertens, A. Sánchez, Phys. Rev. E 73 (2006) 046605.
[20] F.G. Mertens, L. Morales-Molina, A.R. Bishop, A. Sánchez, P. Müller, Phys. Rev. E 74 (2006) 066602.
[21] Y. Zolotaryuk, M. Salerno, Phys. Rev. E 73 (2006) 066621.
[22] E. Zamora-Sillero, N.R. Quintero, F.G. Mertens, Phys. Rev. E 76 (2007) 066601.
[23] A.V. Gorbach, S. Denisov, S. Flach, Opt. Lett. 31 (2006) 1702;
H. Sakaguchi, B.A. Malomed, Physica D 183 (2003) 282.
[24] D. Poletti, T.J. Alexander, E.A. Ostrovskaya, B. Li, Yu.S. Kivshar, Phys. Rev. Lett. 101 (2008) 150403.
[25] L. Khaykovich, F. Schreck, G. Ferrari, T. Bourdel, J. Cubizolles, L.D. Carr, Y. Castin, C. Salomon, Science 296 (2002) 1290.
[26] V.M. Perez-Garcia, H. Michinel, H. Herrero, Phys. Rev. A 57 (1998) 3837.
[27] A.D. Martin, C.S. Adams, S.A. Gardiner, Phys. Rev. Lett. 98 (2007) 020402.
[28] L.D. Faddeev, L.A. Takhtajan, Hamiltonian Methods in the Theory of Solitons, Springer-Verlag, Berlin, Heidelberg, 1987 (Chapter 1).
[29] R. Scharf, A.R. Bishop, Phys. Rev. E 47 (1993) 1375.
[30] M.A. de Moura, J. Phys. A: Math. Gen. 27 (1994) 7157.
[31] L.D. Landau, E.M. Lifshitz, Mechanics, Pergamon, Oxford, 1960.
[32] Yu.S. Kivshar, N. Gronbech-Jensen, R.D. Parmentier, Phys. Rev. E 49 (1994) 4542.
[33] K. Helmerson, M.F. Andersen, C. Ryu, P. Clad, V. Natarajan, A. Vaziri, W.D. Phillips, Nuclear Phys. A 790 (2007) 705c.
[34] T. Salger, C. Geckeler, S. Kling, M. Weitz, Phys. Rev. Lett. 99 (2007) 190405.